
Divisive Normalization from Wilson-Cowan Dynamics

J. Malo^{1,2*}, J.J. Esteve-Taboada², M. Bertalmío³

1 Image Processing Lab., Univ. València, Spain

2 Dept. d'Òptica i Optometria i Ciències de la Visió, Univ. València, Spain

3 Information and Communication Technologies Dept., Univ. Pompeu Fabra, Barcelona, Spain

* Correspondence: jesus.malo@uv.es

Abstract¹

Divisive Normalization and the Wilson-Cowan equations are influential models of neural interaction and saturation [Carandini and Heeger Nat.Rev.Neurosci. 2012; Wilson and Cowan Kybernetik 1973]. However, they have not been analytically related yet. In this work we show that Divisive Normalization can be obtained from the Wilson-Cowan model. Specifically, assuming that Divisive Normalization is the steady state solution of the Wilson-Cowan differential equation, we find that the kernel that controls neural interactions in Divisive Normalization depends on the Wilson-Cowan kernel but also has a signal-dependent contribution. A standard stability analysis of a Wilson-Cowan model with the parameters obtained from our relation shows that the Divisive Normalization solution is a stable node. This stability demonstrates the consistency of our steady state assumption, and is in line with the straightforward use of Divisive Normalization with time-varying stimuli.

The proposed theory provides a physiological foundation (a relation to a dynamical network with fixed wiring among neurons) for the functional suggestions that have been done on the need of signal-dependent Divisive Normalization [e.g. in Coen-Cagli et al., PLoS Comp.Biol. 2012]. Moreover, this theory explains the modifications that had to be introduced ad-hoc in Gaussian kernels of Divisive Normalization in [Martinez et al. Front. Neurosci. 2019] to reproduce contrast responses. The proposed relation implies that the Wilson-Cowan dynamics also reproduces visual masking and subjective image distortion metrics, which up to now had been mainly explained via Divisive Normalization. Finally, this relation allows to apply to Divisive Normalization the methods which up to now had been developed for dynamical systems such as Wilson-Cowan networks.

¹This work expands the original report presented at MODVIS 2018: "Appropriate kernels for Divisive Normalization explained by Wilson-Cowan equations" <https://arxiv.org/abs/1804.05964>

1 Introduction

A number of perceptual experiences in different modalities can be described with the Divisive Normalization interaction among the outputs of linear sensors [1]. In particular, in vision, the perception of color, texture and motion seem to be mediated by this interaction [2–4].

The discussion on the circuits underlying the Divisive Normalization in [1] suggests that there may be different architectures leading to this specific computation. Recent results suggest specific mechanisms for Divisive Normalization in certain situations [5], but the general debate on the physiological implementations that may occur is still open. On the other hand, a number of functional advantages suggest that the kernel that describes the interaction in Divisive Normalization should be adaptive (i.e. signal or context dependent) [6–9]. Moreover, the match between the linear receptive fields and the interaction kernel in the Divisive Normalization is not trivial: the conventional Gaussian kernels in [3, 10] had to be tuned by hand to reproduce contrast responses [11].

These open questions imply that it is interesting to relate Divisive Normalization to other models of neural interaction for a better understanding of its implementation, the structure of the interaction kernel, and its dependence with the signal. Interesting possibilities to consider are the classical neural field models of Wilson-Cowan [12, 13] or Amari [14], which are subtractive in nature.

Subtractive and divisive adaptation models have been qualitatively related before [15, 16]. Both models have been shown to have similar advantages in information-theoretic terms: univariate local histogram equalization in Wilson-Cowan [17] and multivariate probability density factorization in Divisive Normalization [10, 18]. Additionally, both models provide similar descriptions of pattern discrimination [15, 19]. However, despite all these similarities, no direct analytical correspondence has been established between these models yet.

In this paper, we assume that the psychophysical behavior described by Divisive Normalization comes from underlying neural interactions that follow the Wilson-Cowan equation. In particular, we identify the Divisive Normalization response with the stationary regime of a Wilson-Cowan system. From this identification we derive an expression for the Divisive Normalization kernel in terms of the interaction kernel of the Wilson-Cowan equation.

Our theoretical relation has interesting consequences:

(1) The proposed theory provides a physiological foundation (a relation to a dynamical system with fixed wiring among neurons) for the functional suggestions that have been done on the need of signal-dependent Divisive Normalization, e.g. in [8].

(2) It explains the modifications that had to be introduced ad-hoc in the kernel of Divisive Normalization in [11] to reproduce contrast responses. This implies that the Wilson-Cowan dynamics reproduce visual masking, which up to now had been mainly explained via Divisive Normalization (e.g. [3]).

(3) The response of Divisive Normalization to natural images using hand-crafted kernels to reproduce contrast masking coincides with the response obtained using the kernel theoretically deduced from the proposed relation. This implies that the Wilson-Cowan model also predicts subjective image quality, which up to now had been mainly explained via Divisive Normalization, e.g. [10, 20, 21].

(4) A standard stability analysis of a Wilson-Cowan model with the parameters obtained from our relation shows that the Divisive Normalization solution is a stable node. The robustness of Divisive Normalization found through this analysis (which up to now was only usual in dynamic models like Wilson-Cowan [22]) shows the consistency of our steady state assumption. Moreover, this stability is in line with the straightforward use of Divisive Normalization with time-varying stimuli, e.g. as in [4].

The structure of the paper is as follows. The *Materials and Methods* section introduces the notation of the cortical interaction models we are considering: the Divisive Normalization and the Wilson-Cowan equation. We also review the general context in which both models will be applied: the retina-V1 neural path and the perception of contrast of visual patterns. Besides, we recall some experimental facts that will be used to illustrate the performance of the proposed relation: (1) contrast responses curves imply certain interactions between subbands [3, 23], (2) the Divisive Normalization kernel must have a specific structure (identified

in [11]) to reproduce contrast response curves, and (3) the shape of the Divisive Normalization kernel has a specific dependence with the surrounding signal [24]. In the *Results* section we derive the analytical relation between the Divisive Normalization and the Wilson-Cowan equation. The *Discussion* section analyzes the mathematical properties and the perceptual consequences of the proposed relation. First, we check the convergence of the Wilson-Cowan solution to the Divisive Normalization response. Moreover, we demonstrate the consistency of the steady state assumption by showing that the Divisive Normalization is a stable node of the Wilson-Cowan system. Then, we address contrast perception facts using the proposed relation to build a psycho-physically meaningful Wilson-Cowan model: we theoretically derive the specific structure of the kernel that was previously empirically inferred, we show that the proposed interaction kernel adapts with the signal, and as a result, we reproduce general trends of contrast response curves. Finally, we discuss the use of the derived kernel in predicting the metric in the image space.

2 Materials and Methods

In this work the theory is illustrated in the context of models of the retina-cortex pathway. The considered framework follows the program suggested in [1]: a cascade of four isomorphic linear+nonlinear modules. These modules address brightness, contrast, frequency filtered contrast masked in the spatial domain, and orientation/scale masking. An example of the transforms of the input in such models is shown in Fig. 1.

In this general context we focus on the cortical layer: a set of linear sensors with wavelet-like receptive fields modelling simple cells in V1, and the nonlinear interaction between the responses of these linear sensors. Divisive Normalization is the conventional model for the nonlinearities to describe contrast perception psychophysics [3], but here we will explore the equivalent Wilson-Cowan model in the contrast perception context.

Below we introduce the notation of both interaction models and the contrast response facts that have to be explained by the models.

2.1 Modelling cortical interactions.

In the case of the V1 cortex, we refer to the set of responses of a population of simple cells as the vector \mathbf{y} . The considered models (Divisive Normalization and Wilson-Cowan) define a nonlinear mapping that transforms the input vector \mathbf{y} (before the interaction among neurons) into the output vector \mathbf{x} (after the interaction),

$$\mathbf{y} \xrightarrow{\mathcal{N}} \mathbf{x} \quad (1)$$

In this setting, responses are called *excitatory* or *inhibitory*, depending on the corresponding *sign* of the signal: $\mathbf{y} = \text{sign}(\mathbf{y})|\mathbf{y}|$, and $\mathbf{x} = \text{sign}(\mathbf{x})|\mathbf{x}|$. The map \mathcal{N} is an adaptive saturating transform, but it preserves the sign of the responses (i.e. $\text{sign}(\mathbf{x}) = \text{sign}(\mathbf{y})$). Therefore, the models care about cell activation (the modulus $|\cdot|$) but not about the excitatory or inhibitory nature of the sensors (the $\text{sign}(\cdot) = \pm$).

We will refer to as the *energy* of the input responses to the vector $\mathbf{e} = |\mathbf{y}|^\gamma$, where this is an element-wise exponentiation of the amplitudes $|y_i|$.

Given the sign-preserving nature of the nonlinear mapping, for the sake of simplicity in notation, in the rest of the paper the variables \mathbf{y} and \mathbf{x} refer to the activations $|\mathbf{y}|$ and $|\mathbf{x}|$.

2.2 The Divisive Normalization model

Forward transform. The input-output transform in the Divisive Normalization is:

$$\mathbf{x} = \mathbb{D}_{\mathbf{k}} \cdot \mathbb{D}_{(\mathbf{b} + \mathbf{H} \cdot \mathbf{e})}^{-1} \cdot \mathbf{e} \quad (2)$$

where the output vector of nonlinear activations in V1, \mathbf{x} , depends on the energy of the input linear wavelet responses, \mathbf{e} , which are dimension-wise normalized by a sum of neighbor

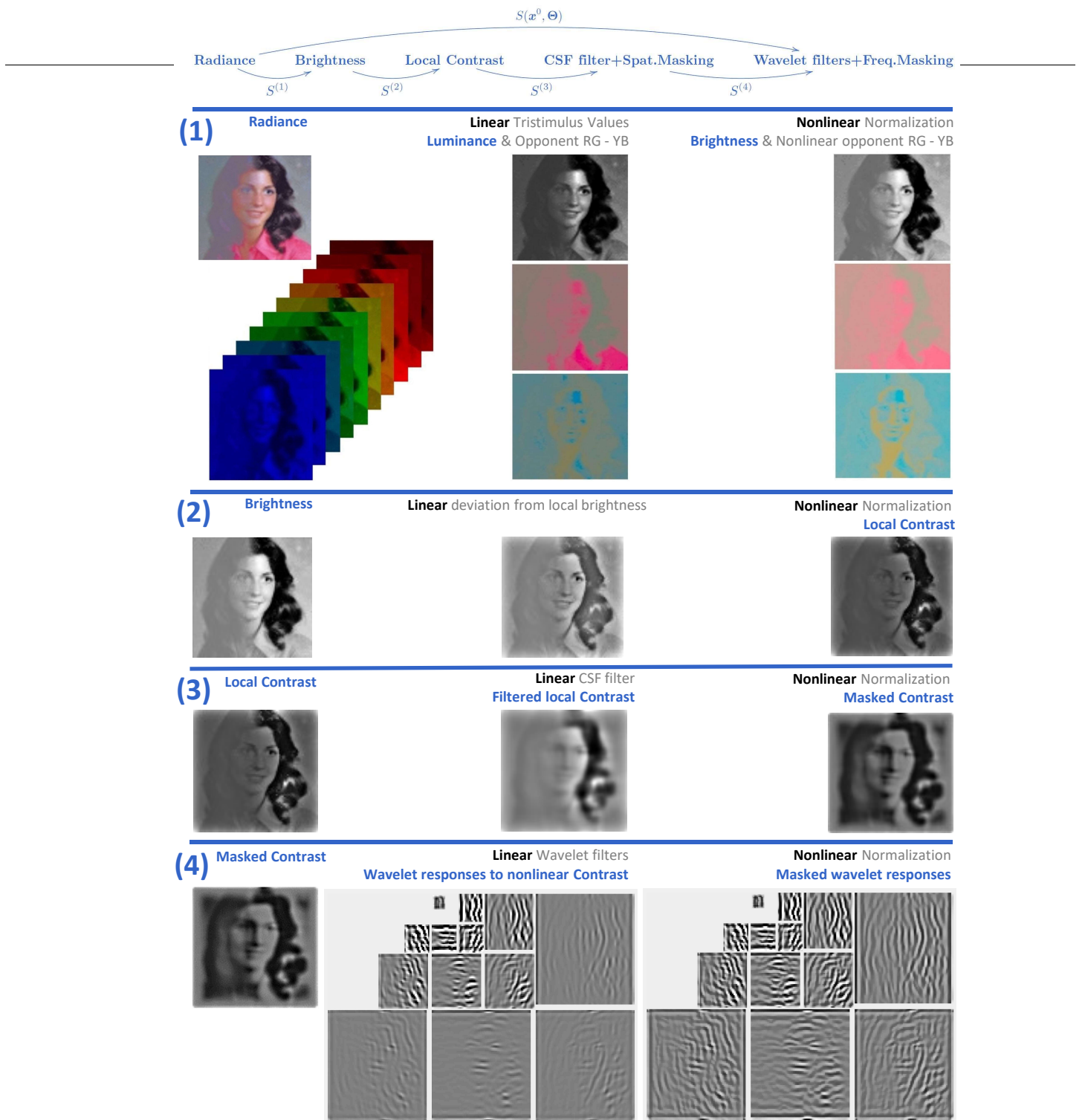


Fig 1. Signal transforms in the retina-cortex pathway: a cascade of L+NL modules. The input is the spatial distribution of the *spectral irradiance* at the retina. For this illustration we modified an image from the USC-SIPI Database [25] to reduce the contrast at the left part of the stimulus. (1) The linear part of the first layer consist of three tristimulus values in each spatial location: one of them is proportional to the luminance, and the other two have opponent chromatic meaning (red-green and yellow-blue). These linear tristimulus responses undergo adaptive saturation transforms. Perception of *brightness* is mediated by an adaptive Weber-like nonlinearity applied to the luminance at each location. This nonlinearity enhances the response in the regions with small linear input (low luminance). (2) The linear part of the second layer computes the deviation of the brightness at each location from the local brightness. Then, this deviation is nonlinearly normalized by the local brightness to give the local nonlinear contrast. (3) The responses to local contrast are convolved by center surround receptive fields (or filtered by the Contrast Sensitivity Function). Then the linearly filtered contrast is nonlinearly normalized by the local contrast. Again normalization increases the response in the regions with small input (low contrast). (4) After linear wavelet transform, each response is normalized by the activity of the neurons in the surround. Again, the activity relatively increases in the regions with low input. The common effect of the nonlinear modules throughout the network is response equalization.

energies. The non-diagonal nature of the interaction kernel \mathbf{H} in the denominator, $\mathbf{b} + \mathbf{H} \cdot \mathbf{e}$, implies that the i -th element of the response may be attenuated if the activity of the neighbor sensors, e_j with $j \neq i$, is high. Each row of the kernel \mathbf{H} describes how the energies of the neighbor simple cells attenuate the activity of each simple cell after the interaction. The each element of the vectors \mathbf{b} and \mathbf{k} respectively determine the semisaturation and the dynamic range of the nonlinear response of each sensor.

Inverse transform. The relation between the two models is easier to obtain by identifying the corresponding decoding transforms in both models. In the case of the Divisive Normalization, the analytical inverse is [18, 26]:

$$\mathbf{e} = (\mathbf{I} - \mathbb{D}_{\mathbf{k}}^{-1} \cdot \mathbb{D}_{\mathbf{x}} \cdot \mathbf{H})^{-1} \cdot \mathbb{D}_{\mathbf{b}} \cdot \mathbb{D}_{\mathbf{k}}^{-1} \cdot \mathbf{x} \quad (3)$$

2.3 The Wilson-Cowan model

Dynamical system. In the Wilson-Cowan model the variation of the activation vector, $\dot{\mathbf{x}}$, increases with the energy of the input, \mathbf{e} , but, for each sensor, this variation is also moderated by its own activity and by a linear combination of the activities of the neighbor sensors,

$$\dot{\mathbf{x}} = \mathbf{e} - \mathbb{D}_{\alpha} \cdot \mathbf{x} - \mathbf{W} \cdot f(\mathbf{x}) \quad (4)$$

where \mathbf{W} is the matrix that describes the damping factor between sensors, and $f(\mathbf{x})$ is a dimension-wise saturating nonlinearity. \mathbf{W} is usually considered to be a fixed matrix made of Gaussian neighborhoods that represent the local interaction between sensors [27]. Note that in Eq. 4 both the inhibitory and the excitatory responses are considered just as negative and positive components of the same vector. Therefore, the two equations in the traditional Wilson-Cowan formulation are represented here by a single expression [28].

Steady state and inverse. The stationary solution of the above differential equation, $\dot{\mathbf{x}} = 0$ in Eq. 4, leads to the following decoding (input-from-output) relation:

$$\mathbf{e} = \mathbb{D}_{\alpha} \cdot \mathbf{x} + \mathbf{W} \cdot f(\mathbf{x}) \quad (5)$$

The identification of the decoding equations in both models, Eq. 3 and Eq. 5, is the key to obtain simple analytical relations between their parameters,

2.4 Experimental facts

2.4.1 Adaptive contrast response curves

In the considered spatial vision context, the models should reproduce the fundamental trends of contrast perception. First, the slope of the contrast response curves depends on the frequency so that the sensitivity at threshold contrast is different for different frequencies according to the Contrast Sensitivity Function [29]. Second, the response curves saturate with contrast [30, 31]. Finally, the responses attenuate with the energy of the background or surround, and this additional saturation depends on the texture of the background [3, 32]: if the test is similar to the background in frequency/orientation decay is stronger. This background-dependent adaptive saturation, or *masking*, is mediated by cortical sensors tuned to spatial frequency with responses that saturate depending on the background as illustrated in Fig. 2.

The above trends are key to discard too simple models and to propose the appropriate modifications in the architecture to get reasonable models [11].

2.4.2 Unexplained kernel structure in Divisive Normalization

In the Divisive Normalization setting, the masking interaction between tests and backgrounds of different texture is classically described by using a Gaussian kernel in the denominator of Eq. 2 in wavelet-like domains: the effect of the j -th wavelet sensor on the attenuation of the i -th wavelet sensor decays with the distance in space, frequency and orientation [3]. We will

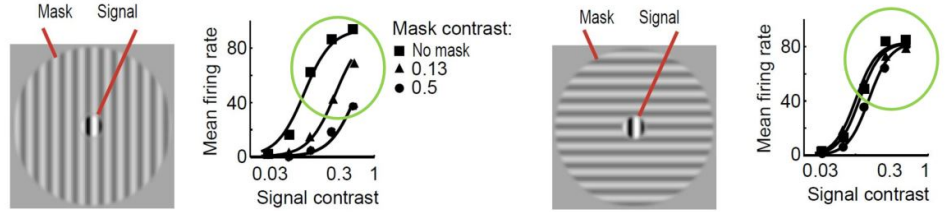


Fig 2. Illustrative contrast response curves. Mean firing rate (response) of V1 neurons tuned to the test as a function of the test contrast in two masking situations (adapted from [23,33]). Note the decay in the response when test and mask do have the same spatio-frequency characteristics, as opposed to the case where they do not (difference in the curves highlighted by the circles in green).

refer to these unit-norm Gaussian kernels as \mathbf{H}^{ws} or Watson and Solomon kernels [3]. Gaussian kernels are useful to describe the general behavior in Fig. 2: activity in close neighbors lead to strong decays in the response while activity in neighbors tuned to more distant features has smaller effect.

However, in order to have well behaved responses in every subband with every possible background, a *special balance* between the wavelet representation and the Gaussian kernels is required. In [11] we found that classical unit-norm Gaussian kernels require *ad-hoc* extra modulation to avoid excessive effect of low frequency backgrounds on high frequency tests.

When using reasonable log-polar Gabor basis or steerable filters to model V1 receptive fields as in [3,33] the energies of the units tuned to low frequencies is notably higher than the energy of high-frequency sensors. Moreover, the smaller number of sensors in low frequency subbands in this kind of wavelet representations implies that unit-norm Gaussian kernels have bigger values in coarse subbands. These two facts overemphasize the impact of low-frequency responses on high-frequency responses. The appropriate wavelet-kernel balance was reestablished by introducing extra high-pass filters in the Gaussian kernel, \mathbf{H}^{ws} , to moderate the effect of low frequencies [11]:

$$\mathbf{H} = \mathbb{D}_l \cdot \mathbf{H}^{ws} \cdot \mathbb{D}_r \quad (6)$$

While the diagonal matrix at the right, \mathbb{D}_r , pre-weights the subbands of \mathbf{e} to moderate the effect of low frequencies before computing the interaction; the diagonal matrix at the left, \mathbb{D}_l , tunes the relative weight of the masking for each sensor, moderating low frequencies again. The vectors \mathbf{r} and \mathbf{l} were tuned by hand in [11] to get reasonable contrast response curves both for low frequency tests and high frequency tests.

The Supplementary Material 6.1 summarizes the results in [11], where different cortical Divisive Normalizations were considered, and shows the differences between the classical unit-norm kernel and the kernel with appropriate high-pass modulation given by Eq. 6. In [11] we pointed out the need of this specific structure in the Divisive Normalization kernel (extra diagonal high-pass filters in Eq. 6) based on empirical grounds, and proposed a procedure to tune these high-pass filters to lead to reasonable contrast response curves.

However, *what is the explanation for this specific structure of the kernel in Eq. 6? Where these two high-pass diagonal matrices come from?*

2.4.3 Adaptive nature of kernel in Divisive Normalization

Experimental results [23] imply that masking interactions are not fixed, but they depend on the context (see Fig. 3 -data-). Statistical explanations have been proposed for this behavior [34] (see Fig. 3 -statistical model-), but no specific mechanism was proposed to describe how this adaptation in the kernel may be implemented.

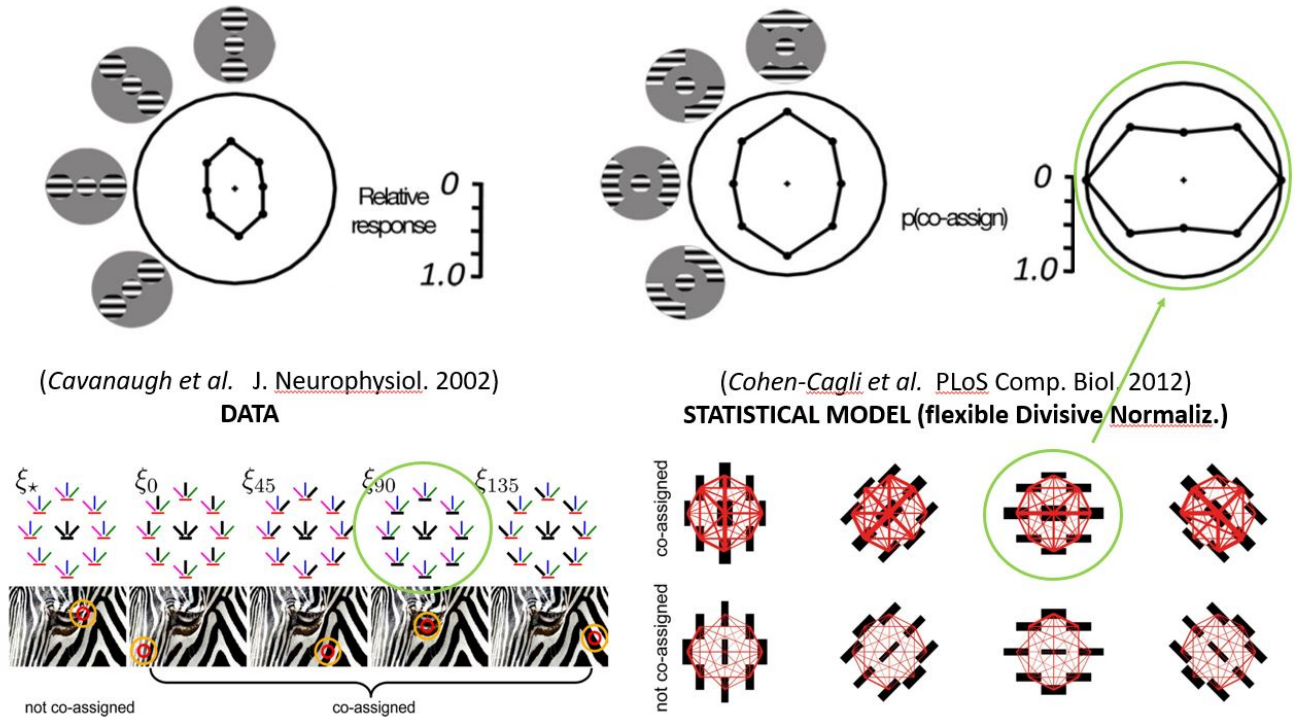


Fig 3. Adaptation of kernel from Cavanaugh and corresponding statistical model from Coen-Cagli (adapted from [34]).

3 Result: analytical equivalence between models

The kernels that describe the relation between sensors in the Divisive Normalization and the Wilson-Cowan models, \mathbf{H} and \mathbf{W} , have similar qualitative roles: both moderate the response either by division or subtraction. Here we derive the equivalence between both models assuming that the Divisive Normalization behavior is the steady state solution of the Wilson-Cowan dynamics. This leads to an interesting analytical relation between \mathbf{H} and \mathbf{W} .

Under the steady state assumption, we can identify the decoding equations in both cases: Eq. 3 and Eq. 5. However, just to get a simpler analytical relation between the kernels, we make one extra assumption on each model.

First, in the Divisive Normalization model, the identification is simpler by taking the series expansion of the inverse in Eq. 3. This expansion was used in [18] because it clarifies the condition for invertibility:

$$(I - \mathbb{D}_k^{-1} \cdot \mathbb{D}_x \cdot \mathbf{H})^{-1} = I + \sum_{n=1}^{\infty} (\mathbb{D}_k^{-1} \cdot \mathbb{D}_x \cdot \mathbf{H})^n$$

The inverse exist if the eigenvalues of $\mathbb{D}_k^{-1} \cdot \mathbb{D}_x \cdot \mathbf{H}$ are smaller than one so that the series converges. In fact if the eigenvalues are small, the inverse can be well approximated by a small number of terms in the series.

$$\begin{aligned} e &= \mathbb{D}_b \cdot \mathbb{D}_k^{-1} \cdot \mathbf{x} + (\mathbb{D}_k^{-1} \cdot \mathbb{D}_x \cdot \mathbf{H}) \cdot \mathbb{D}_k^{-1} \cdot \mathbb{D}_b \cdot \mathbf{x} + \\ &\quad + (\mathbb{D}_k^{-1} \cdot \mathbb{D}_x \cdot \mathbf{H})^2 \cdot \mathbb{D}_k^{-1} \cdot \mathbb{D}_b \cdot \mathbf{x} + \\ &\quad + (\mathbb{D}_k^{-1} \cdot \mathbb{D}_x \cdot \mathbf{H})^3 \cdot \mathbb{D}_k^{-1} \cdot \mathbb{D}_b \cdot \mathbf{x} + \dots \end{aligned}$$

$$e \approx (\mathbb{D}_b \cdot \mathbb{D}_k^{-1} + \mathbb{D}_k^{-1} \cdot \mathbb{D}_x \cdot \mathbf{H} \cdot \mathbb{D}_b \cdot \mathbb{D}_k^{-1}) \cdot \mathbf{x} \quad (7)$$

Second, in the case of the Wilson-Cowan model, in Eq. 5 we approximate the saturation function by means of the first derivative (green function in Fig.4, left): $f(\mathbf{x}) \approx \mathbb{D}_f \cdot \mathbf{x}$. As a

result, Eq. 5 can be written as:

$$\mathbf{e} = (\mathbb{D}_\alpha + \mathbf{W} \cdot \mathbb{D}_f) \cdot \mathbf{x} \quad (8)$$

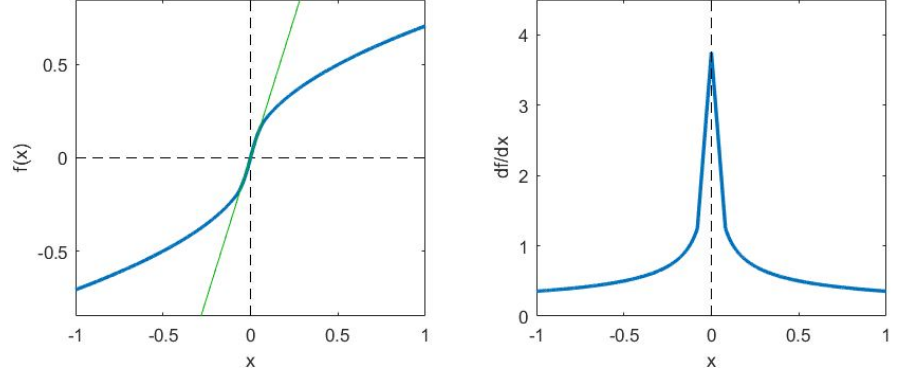


Fig 4. Saturation in Wilson-Cowan model. (left) Saturating function in blue and linear approximation around the origin in green. (right) Derivative of the saturating function decreases with amplitude.

Now, the identification between the simplified versions of the decoding equations, Eq. 7 and Eq. 8, is straightforward. As a result, we get the following relations between the parameters of both models:

$$\begin{aligned} \mathbf{b} &= \mathbf{k} \odot \alpha \\ \mathbf{H} &= \mathbb{D}_{\left(\frac{\mathbf{k}}{\alpha}\right)} \cdot \mathbf{W} \cdot \mathbb{D}_{\left(\frac{\mathbf{k} \odot \mathbf{f}}{\mathbf{b}}\right)} \end{aligned} \quad (9)$$

Both models are equivalent if the Divisive Normalization kernel inherits the structure from the Wilson-Cowan kernel modified by these pre- and post-diagonal matrices. Note that the resulting \mathbf{H} in Eq. 9 has exactly the structure in Eq. 6. This theoretical result suggests an explanation for the structure that had to be introduced ad-hoc in [11] just to reproduce contrast masking (see Supplementary Material 6.1). Note that interaction in the Wilson-Cowan case may be understood as wiring between sensors tuned to similar features, so unit-norm Gaussian, $\mathbf{W} = \mathbf{H}^{ws}$, is a reasonable choice [13, 27]. Note also that the weights before and after the Gaussian interaction (the diagonal matrices) are signal dependent, which implies that the interaction kernel in Divisive Normalization should be *adaptive*. The one in the left has a direct dependence on the inverse of the signal, while the one in the right depends on the derivative, which also depends on the signal as seen in Fig. 4, right. In the next Section we show that the vectors (Hadamard quotients) \mathbf{k}/α and $\mathbf{k} \odot \mathbf{f}/\mathbf{b}$ do have the high-pass frequency nature that explains why the low frequencies in \mathbf{e} had to be attenuated by \mathbf{r} and \mathbf{l} . We also show that the term of the right produces the shape changes needed on the interactions.

It is important to stress that the assumptions made to get the simplified versions of the decoding equations that lead to the analytical relations in Eq. 9, were done only for the sake of simplicity in the final relations obtained. Actually, once these relations were obtained, the simulations in the following sections use the full expressions of the models (i.e. no linearization or truncation is assumed any more). In summary, the relations in Eq. 9 are exact for simplified versions of the models and only an approximation for the full versions of the models. However, the discussion below points out the validity of this approximation since plugging these expressions into the full versions of the models also leads to consistent results.

4 Discussion

Here we analyze the mathematical properties and perceptual consequences of the proposed relation between models, Eq. 9. First, we prove the consistency of the steady state assumption by showing that (a) the integration of the Wilson-Cowan equation converges to the Divisive Normalization solution, and (b) the Divisive Normalization solution is a stable node of the

Wilson-Cowan system. Convergence and stability results are obtained with sensible parameters for the visual cortex since they were psychophysically tuned in [11, 26, 35]. Then, we address different aspects of contrast perception using Wilson-Cowan and the proposed relation: (a) we analyze the signal-dependent behavior of the theoretically derived kernel in natural images and the benefits of the high-pass behavior to moderate the weight of the low-frequency components; (b) we show that the shape of the interactions between sensors changes depending on the surround; (c) we reproduce the contrast response curves with the proposed signal-dependent kernel; and (d) we discuss the use of the derived kernel in predicting the subjective metric of the image space.

4.1 Mathematical properties

4.1.1 Convergence to the Divisive Normalization solution

The Wilson-Cowan expression defines an initial value problem where the response at time zero evolves (or is updated) according to the right hand side of the differential Eq. 4. In our case, we assume that the initial value of the output response is just the input e . Then, we propagate this solution through simple Euler integration.

Figure 5 shows the evolution of the response from this integration using auto-attenuation and interaction values, α and \mathbf{W} , compatible with the psychophysical experiments in [11, 26, 35]. Results shows that, with these parameters applied to 35 natural images taken from calibrated databases [36, 37], the solution of the Wilson-Cowan integration converges to the Divisive Normalization solution. Note that the difference between both solutions decreases as the Wilson-Cowan response is updated (Fig.5, right), and this result is the steady state because the update in the solution tends to zero (Fig.5, left). The final relative difference between the steady state of the Wilson-Cowan integration and the Divisive Normalization solution is $\frac{|x_{WC} - x_{DN}|^2}{|x_{DN}|^2} = 0.0011 \pm 0.0004$.

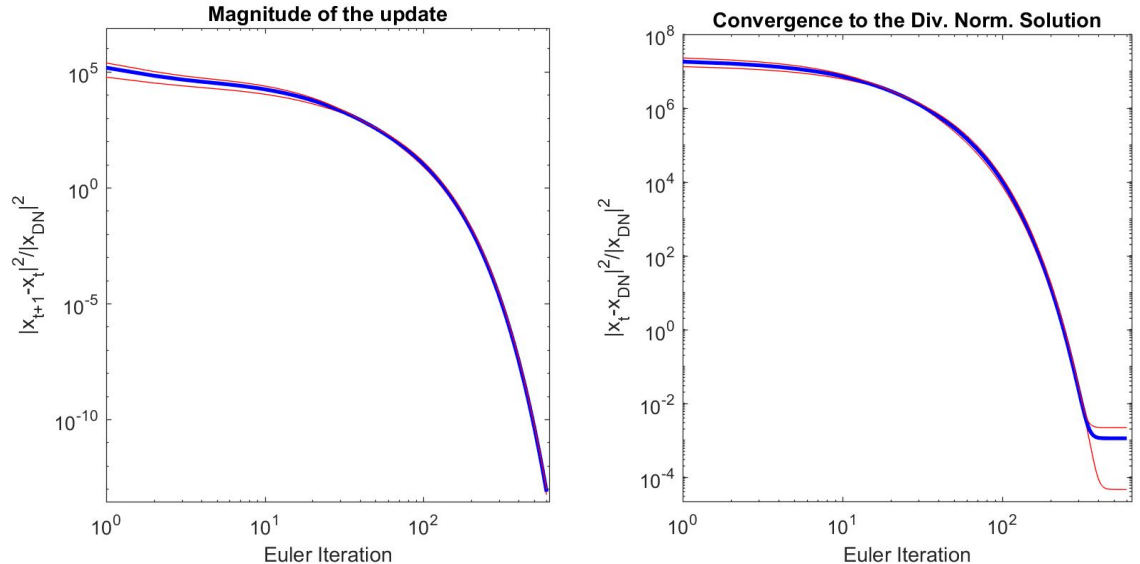


Fig 5. Convergence to the Divisive Normalization solution. *Left:* evolution of the relative energy of the update of the solution along the integration. *Right:* evolution of the relative energy of the difference between the Wilson-Cowan solution and the Divisive Normalization solution along the integration. The curves in blue are the average of the update and difference over 35 natural images, and the intervals in red represent 3 standard deviations below and above the mean.

4.1.2 Stability analysis of Divisive Normalization solution

The Jacobian with regard to perturbations in the output of the right hand side of the differential Eq. 4 determines the stability of a dynamical system: if the eigenvalues of this Jacobian are all negative, the fixed point is a stable node [38].

From the differential equation of the Wilson-Cowan system, Eq. 4, the Jacobian with regard to the output signal is:

$$J = -(\mathbb{D}_\alpha + \mathbf{W} \cdot \mathbb{D}_f) = -(\mathbb{D}_{(b/k)} + \mathbb{D}_{(x/k)} \cdot \mathbf{H} \cdot \mathbb{D}_{(b/k)}) \quad (10)$$

where we also used the proposed relation, Eq. 9, to put the Jacobian in terms of the parameters of the equivalent Divisive Normalization network. In this way, we can use specific experimental values for the (Divisive Normalization) parameters fitted through extensive M^Aximum D^Ifferentiation psychophysics [35], reproduction of subjective quality opinion [26], and to get qualitatively correct contrast response curves [11], reviewed in Supplementary Material 6.1.

Qualitative analysis of Eq. 10 anticipates that the eigenvalues of the Jacobian are *all negative*: note that an interaction \mathbf{W} made of unit-norm Gaussian neighborhoods, a positive slope of the activation f , and a positive auto-attenuation α , guarantee that, given the negative sign, all the eigenvalues of J are real and negative.

Below we show quantitative examples of the stability of the system in two situations: (a) an illustrative toy model for 3-pixel images (fully specified in Supplementary Material 6.2) that allows full visualization of the vector field of perturbations in the phase space of the system. and (b) the full-scale model for actual images, with parameters \mathbf{k} , \mathbf{b} and \mathbf{H} fitted in [11, 26, 35].

In the reduced-scale model, perturbations of the response leads to the dynamics shown in the phase space of Fig. 6. The vector field induced by the Jacobian implies that any perturbation is sent back to the origin (no-perturbation) point, which is a stable node of the system.

This behavior is consistent for any response \mathbf{x} as can be seen by plotting the equivalent results using the signal dependent Jacobian (the one that depends on the Divisive Normalization parameters in the right hand side of Eq. 10).

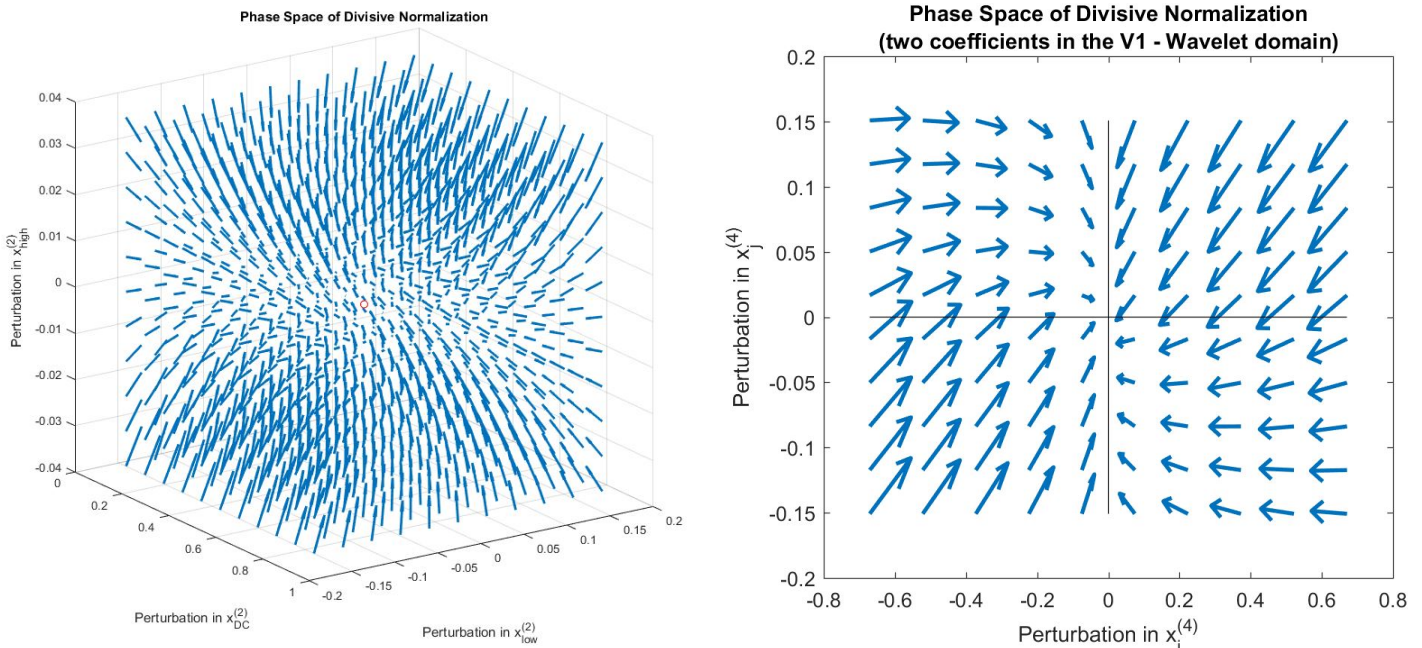


Fig 6. Stability of the Divisive Normalization solution (I). Vector field in the phase space generated by the Jacobian of the reduced-scale Wilson-Cowan model (just 3 sensors). *Left*: evolution of perturbations in the three sensors. *Right*: detail of evolution of perturbations restricted to the plane of sensors tuned to non-zero frequencies.

Fig. 7 shows the dynamics around a range of responses in the non-zero frequency plane for constant value of the sensor tuned to brightness (zero-frequency). In every case, eventual oscillations are attenuated and the response returns to the Divisive Normalization solution highlighted in red. The behavior at other brightness levels is equivalent and perturbations not restricted to the non-zero frequency plane are attenuated as well.

More interestingly, a meaningful full-scale cortical model fitted using visual psychophysics [11, 26, 35] also leads to the same result: the Divisive Normalization solution is a stable node of the equivalent dynamical Wilson-Cowan network. In this full-scale case the phase space cannot

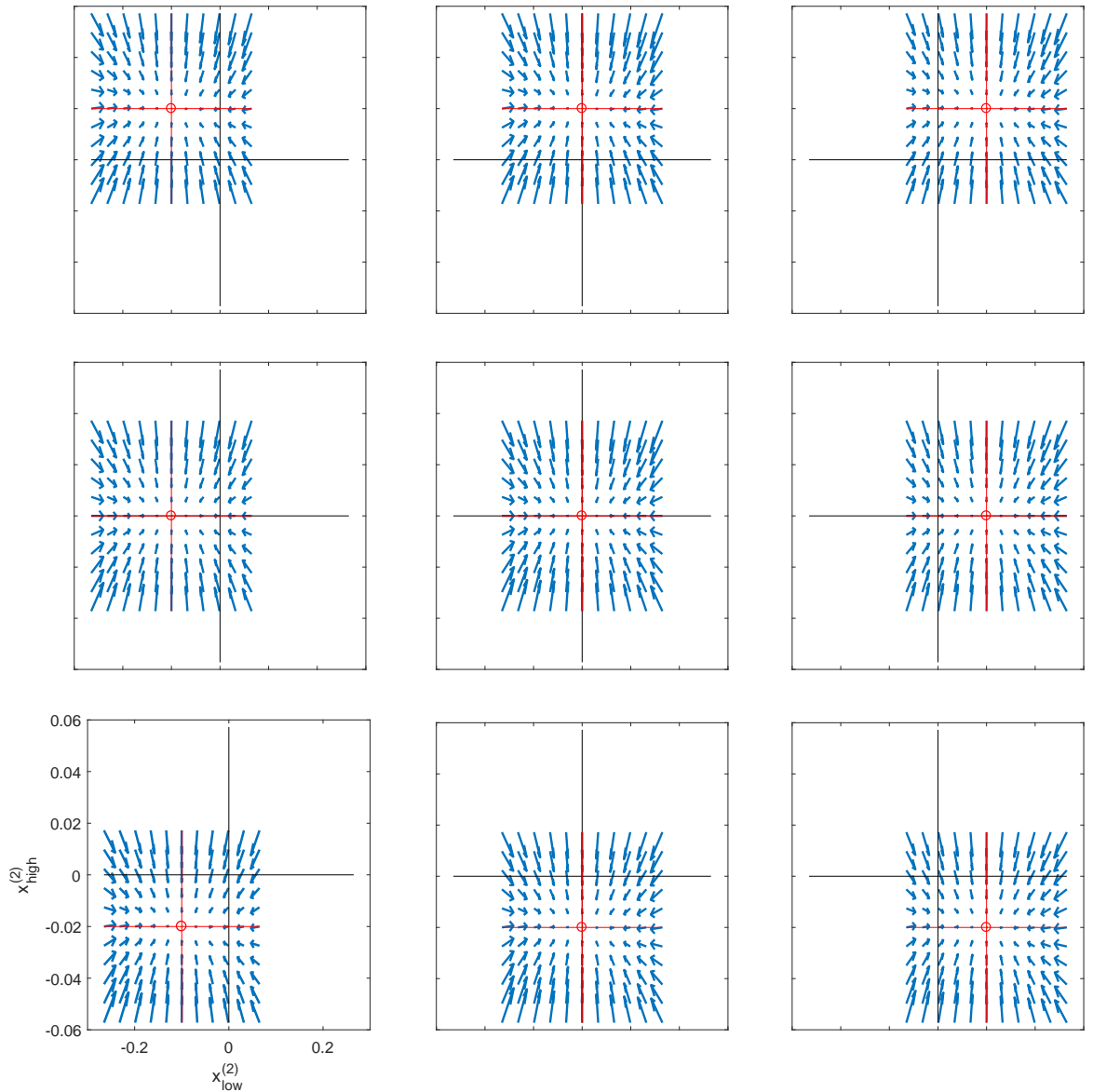


Fig 7. Stability of the Divisive Normalization solution (II). Attenuation of oscillations across the response space in the reduced-scale Wilson-Cowan model. In each plot (non-zero frequency sensors), the point highlighted in red represents a specific Divisive Normalization response which is perturbed along the axes in red. The Jacobian leads to the field that describes the evolution of the dynamic system and attenuates the perturbation towards the original point in red.

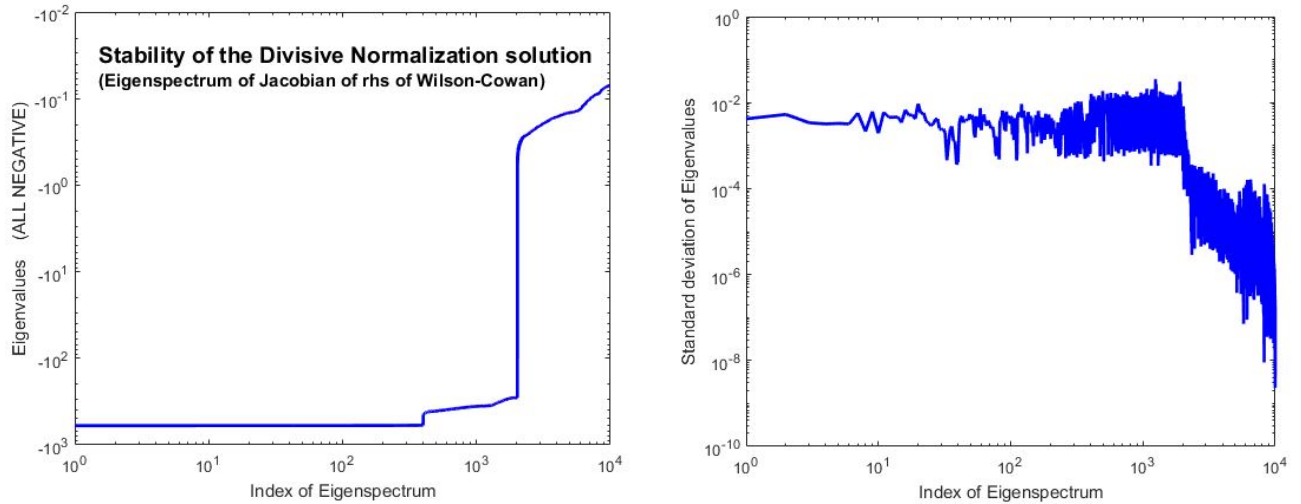


Fig 8. Stability of the Divisive Normalization solution (III). *Left:* Eigenspectrum of the Jacobian of the differential equation with psychophysically tuned parameters is *all negative*, thus the Divisive Normalization is a stable node of the system. *Right:* the variability of the eigenspectrum over natural images is small.

be visualized as above. Therefore, we rely on the analysis of the eigenvalues of the Jacobian computed using Eq. 10 with the experimental parameters for Divisive Normalization shown in Supplementary Material 6.1. In this experiment we evaluated the eigenvalues with responses to 10^5 patches of 40×40 images taken from the calibrated Van Hateren natural image database [36]. Figure 8 shows that *all* the eigenvalues are negative indicating that the Divisive Normalization solution is a stable node of the dynamical system, and that this behavior is consistent (small variance) for the range of responses elicited by natural images. This quantitative check is consistent with the qualitative reasoning done above based on the structure of the kernel and the sign of the parameters of the equation.

The conclusion of this analysis is that realistic Divisive Normalization solutions are stable nodes of the equivalent Wilson-Cowan systems. This conclusion confirms the assumption under the proposed relation (Divisive Normalization as steady state of the Wilson-Cowan dynamics).

4.2 Contrast perception in divisive and subtractive models

The proposed theory implies that the Divisive Normalization kernel inherits the structure of the Wilson-Cowan interaction matrix modified by some specific signal dependent diagonal matrices, Eq. 9. Taking into account that Gaussian neighborhoods have been used for the Wilson-Cowan interaction [13,27], our prediction seems consistent with previous suggestions of required modifications of Gaussian kernels in Divisive Normalization to reproduce contrast perception (see [11] and Supplementary Material 6.1).

Here we first discuss the implications of the predicted signal dependence and show that it actually justifies the modifications that were empirically introduced in the Divisive Normalization kernels. Then, we take the predicted signal-dependent kernel and simulate contrast response curves.

4.2.1 Structure of the kernel in Divisive Normalization

In this section we analyze the effect of the signal, \mathbf{x} , in the Divisive Normalization kernel according to Eq. 9 by using an illustrative stimulus and psychophysically sensible values for the parameters \mathbf{k} , \mathbf{b} and \mathbf{H}^{ws} .

Moreover we compare the empirical filters (vectors \mathbf{l} and \mathbf{r}) presented in [11], Eq. 6, with the corresponding theoretical vectors in Eq. 9. We also compare the masking term in the

denominator of Divisive Normalization using (1) the Gaussian kernel $\mathbf{H}^{ws} \cdot \mathbf{e}$, (2) the empirically modified kernel $\mathbb{D}_l \cdot \mathbf{H}^{ws} \cdot \mathbb{D}_r \cdot \mathbf{e}$, and (3) the theoretically derived kernel obtained from Eq. 9, $\mathbb{D}(\frac{k}{a}) \cdot \mathbf{W} \cdot \mathbb{D}(\frac{k}{b}) \cdot \mathbf{e}$. In this comparison we assume a Gaussian wiring in \mathbf{W} .

Before going into the details of the kernel, let's have a look at the response \mathbf{x} for an illustrative input image. Fig.9 shows the corresponding responses of linear and nonlinear V1-like sensors based on steerable wavelets. Typical responses for natural images are low-pass signals (see the

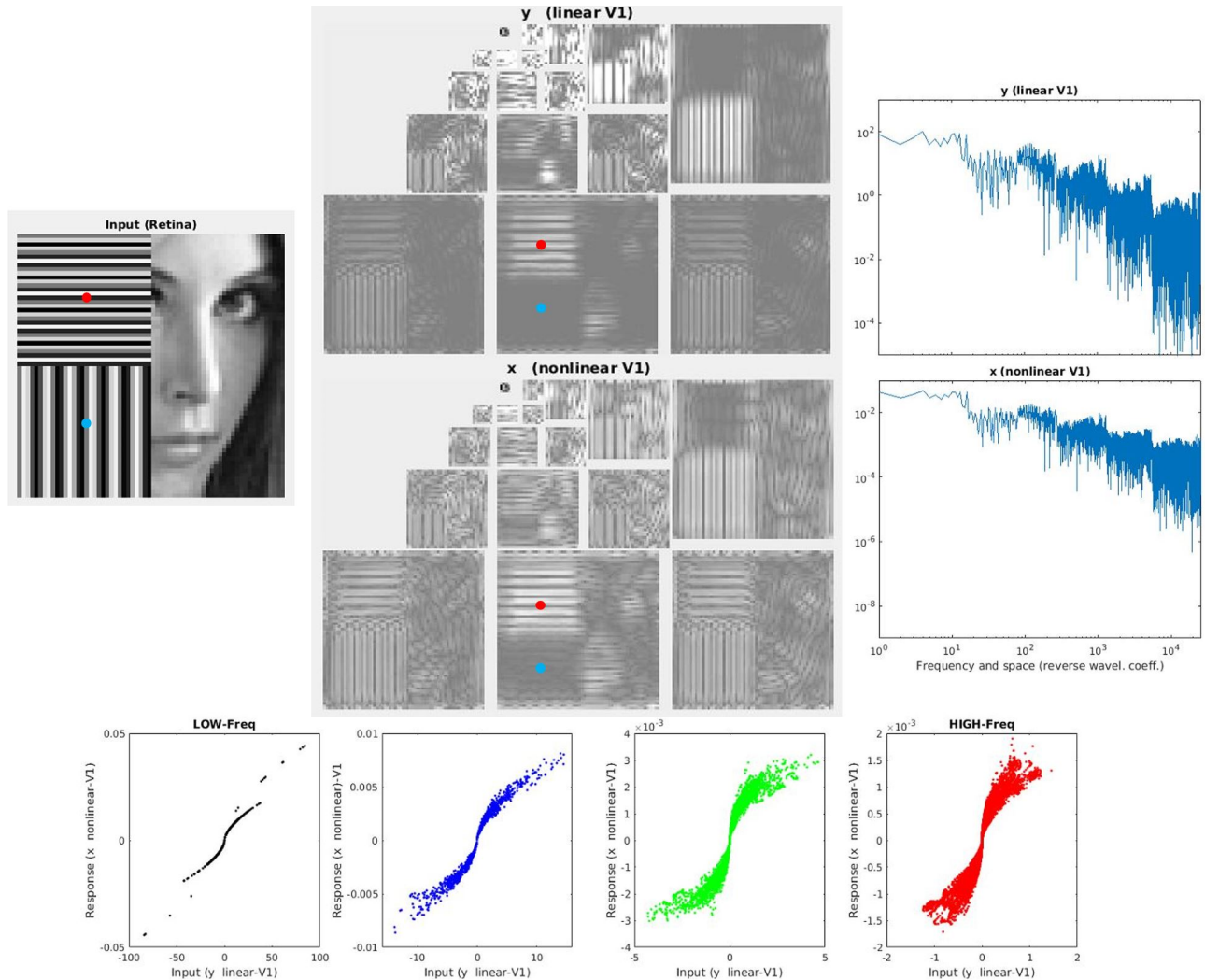


Fig 9. Responses in V1 for an illustrative stimulus. The retinal image (left panel) is composed by a natural image and two synthetic patches of frequencies 12 and 6 cycles per degree (cpd). This image goes through the first stages of the model (see Fig 1) up to the cortical layer where a set of linear wavelet filters lead to the responses \mathbf{y} , with energy \mathbf{e} , which are nonlinearly transformed into the responses \mathbf{x} . Central wavelet panels represent these signals. The plots at the right show the vector representation of the wavelet coefficients flattened according to the MatlabPyrTools convention [39]. These plots show how natural images typically have bigger energy in the low-frequency sensors. Plots at the bottom (from black-to-red) show that Divisive Normalization implies adaptive saturating nonlinearities depending on the neighbors (i.e. a family of sigmoid functions in the input-output scatter plots). The highlighted sensors in red and blue (tuned to different locations of the 12 cpd scale, horizontal orientation) have characteristic responses given the patterns in those locations (see text).

vectors at the right of the corresponding wavelet-like representations). The response in each subband is an adaptive (context dependent) nonlinear transduction. Each point at the black-to-red plots at the bottom represents the input-output relation for each neuron in the subbands of the different scales (from coarse to fine). As each neuron has a different neighborhood there is no simple input-output transduction function, but a scatter plot representing different instances of an adaptive transduction.

The considered image is illustrative since it is designed to lead to specific excitations in certain sensors (subbands and locations in the wavelet domain). Note, for instance, the high and low frequency synthetic patterns (12 and 6 cpd, horizontal and vertical respectively) in the retinal regions with the red and blue points. In the wavelet representations we also highlighted some specific sensors in red and blue corresponding to those spatial locations and the horizontal subband tuned to 12 cpd. Given the tuning properties of the neurons highlighted in red and blue, it makes sense that the sensor in red has bigger response than the sensor in blue.

With this knowledge of the signal in mind (low-pass trend in \mathbf{x} shown in Fig. 9, and also low-pass trend in the semisaturation \mathbf{b} shown in Fig. 15, that summarizes the results in [11]), we can imagine the *high-pass* nature of the vectors $\frac{1}{\mathbf{x}}$ and $\frac{1}{\mathbf{b}}$ that appear at the left and right of the kernel \mathbf{W} in Eq. 9.

Fig. 10 actually compares the empirical *left* and *right* vectors, \mathbf{l} and \mathbf{r} (hand crafted to reproduce contrast curves in [11]), with those based on the proposed relation with the Wilson-Cowan model (vectors based on $\frac{1}{\mathbf{x}}$ and $\frac{1}{\mathbf{b}}$). Interestingly, both empirical and theoretical show similar high-pass nature and coincide in order of magnitude.

Consistency of the structure of the empirical and theoretical kernels (Eq. 6 and Eq. 9),

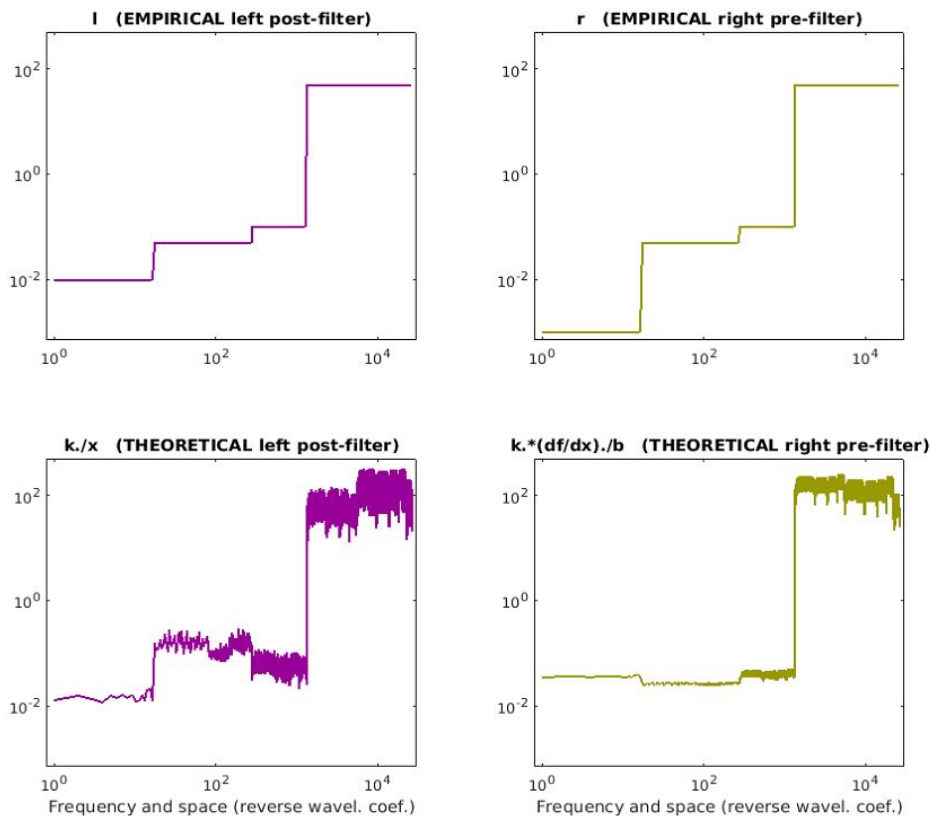


Fig 10. Theoretical and empirical modulation of the Divisive Normalization kernel. Vectors in the left- and right- diagonal matrices that multiply the Gaussian kernel in the empirical tuning represented by Eq. 6 (top) and in the theoretically derived Eq. 9 (bottom).

and coincidence of empirical and theoretical filters (Fig. 10) suggests that the proposed theory explains the modifications in the classical unit-norm kernels required in Divisive Normalization.

4.2.2 Shape adaptation of the kernel depending on the signal

Once we analyzed the high-pass nature of $\mathbb{D}_{(\frac{k}{a})}$ and $\mathbb{D}_{(\frac{k}{b})}$, let's see in more detail the signal-dependent adaptivity of the kernel. In order to do so, let's consider the interaction neighborhood of two particular sensors in the wavelet representation: specifically, the sensors highlighted in red and blue in Fig. 9. In Fig. 11 we compare different versions of the two individual neighborhoods (the two rows of the corresponding kernel matrices) seen in the same wavelet representation. Three cases are considered: (1) the unit-norm Gaussian kernels, \mathbf{H}^{ws} , (2) the empirical kernel modulated by hand-crafted pre and post filters, Eq. 6, and (3) the theoretical kernel that depends on the signal, Eq. 9. In the three diagrams lighter gray in each j -th sensor corresponds to bigger interaction with the considered i -th sensor (highlighted in color). The gray values are normalized to the maximum in each case. Each subband displays two Gaussians. Obviously, each Gaussian corresponds to only one of the sensors (the one highlighted in red or in blue, depending on the spatial location of the Gaussian). We used a single wavelet diagram in each case since the two neighborhoods do not overlap and there is no possible confusion between them.

The first case \mathbf{H}^{ws} at the top of Fig. 11 is the base-line unit-norm (or unit-volume) Gaussian kernel. In this case, in the spatial domain corresponding to each subband, a unit-norm Gaussian in space is defined centered in the sensor tuned to the spatial location preferred by the i -th sensor. Then, the corresponding Gaussians at different scales and orientations are weighted by a factor that decays as a Gaussian over scale and orientation from the maximum, centered at the subband of the i -th sensor. That is why the replicas of the Gaussian highlighted with color fade away across the pyramid.

The *problem* with the unit-norm Gaussian in every scale is that the reduced set of sensors for low-frequency scales lead to higher values of the neighborhood so that they subtend the required volume. In that situation the impact of activity in low-frequency subbands is substantially higher. This combined with the low-pass trend of wavelet signals implies a strong bias of the response and ruins the contrast masking curves. This *problem* is represented by the relatively high values of the neighborhoods in the subbands highlighted in red.

This overemphasis of low frequency was corrected ad-hoc using right- and left- multiplication in Eq. 6 by hand-crafted high-pass filters. This strongly reduces the values for the Gaussian neighborhoods at the low frequency as seen in the empirical kernels at the central diagram. See the positive effect of the high-pass filters in minimizing the impact of the neighborhoods at low frequency (subbands highlighted in green).

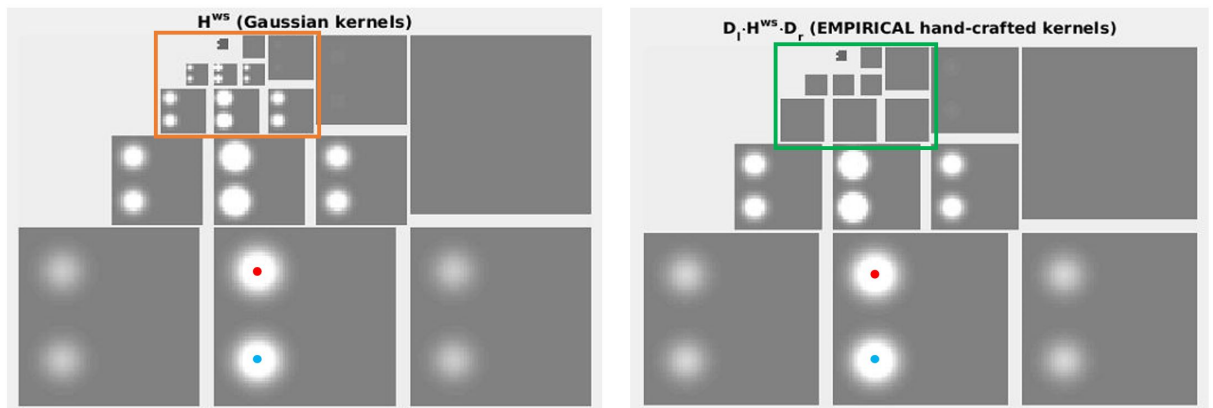


Fig 11. Interaction kernels for the sensors highlighted in red and blue in Fig. 9. Gaussian kernel (left) with overestimated contribution of low frequency (subbands highlighted in orange). Hand-crafted kernel (right) to reduce the influence of low frequencies (see subbands highlighted in green)..

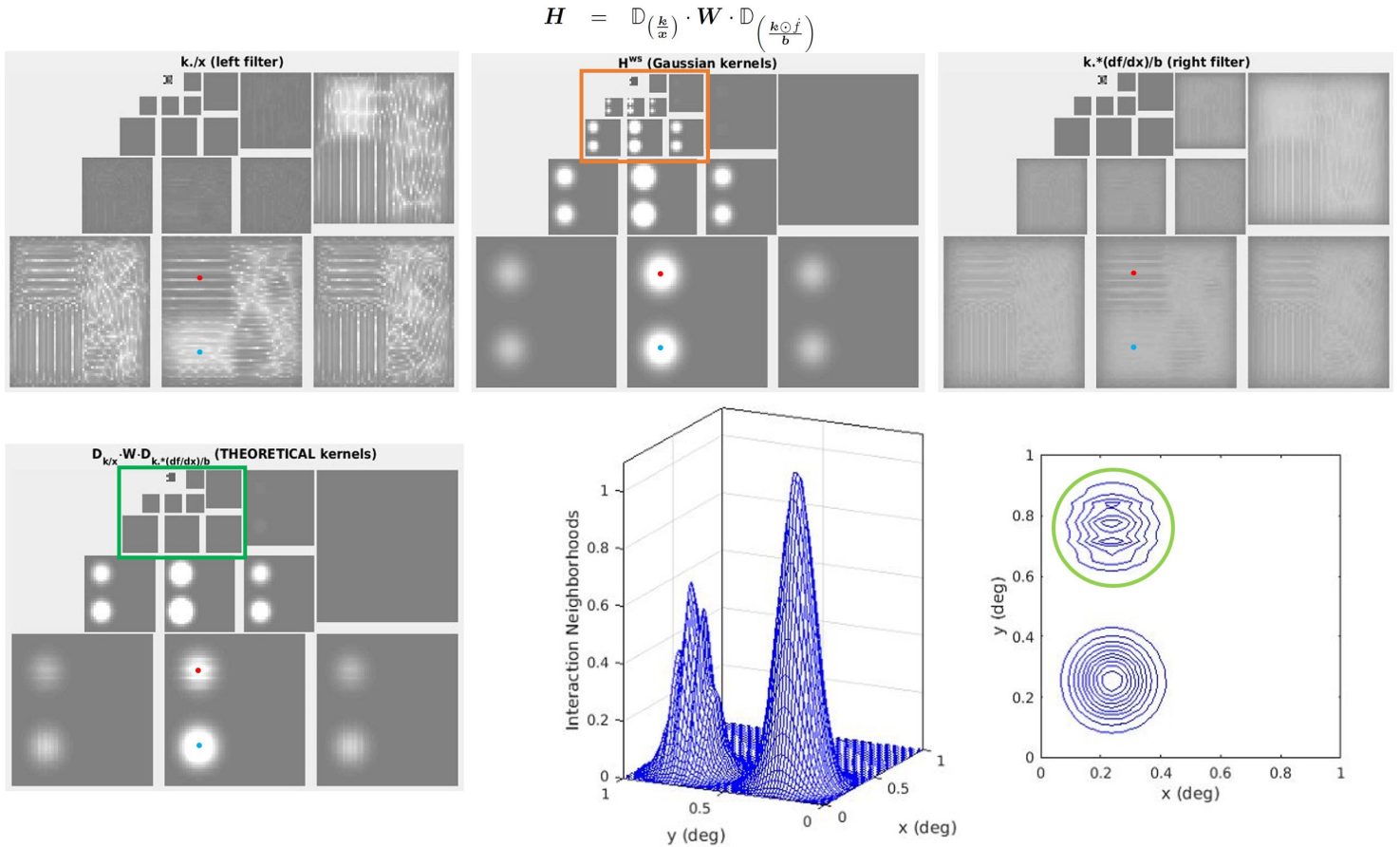


Fig 12. Changes in the shape of the interaction. The proposed relation implies changes of the shape of the kernel (from circular to horizontal ellipse) when the context is a high contrast horizontal pattern. This is compatible with the experimental facts reported above [24].

In both cases (the classical H^{ws} , and the hand-crafted $H = \mathbb{D}_l \cdot H^{ws} \cdot \mathbb{D}_r$, at the top and center) the size of the interaction neighborhood (the interaction length) is signal independent. Note that the neighborhoods for both sensors (red and blue) are the same regardless of the different stimulation that can be seen in Fig. 9.

The kernels at the bottom are those obtained from Eq. 9. These theoretically-derived kernels remove the bias due to the low frequencies just as the hand-crafted kernel (see the subbands highlighted in green), but also introduce an extra signal dependence. Note that the interaction neighborhood now depends on the location (bigger for the sensor in blue) due to the different value of the signal: lower response for this sensor implies, through $\frac{1}{x}$, an increased interaction with the neighbors. In this way, the interaction length would depend on the response.

Finally, we show how the proposed relation implies that the shape of the interaction kernel depends on the context (see Fig. 12).

In summary, deriving the Divisive Normalization as the steady state of a Wilson-Cowan system with Gaussian wiring explains the high-pass filters that had to be added recently to the structure of the kernel in Divisive Normalization to solve problems of the classical Gaussian kernel (in Divisive Normalization). Moreover, this relation also suggest that the interaction length between sensors in the Divisive Normalization model should depend on the input.

4.2.3 Response curves from Wilson-Cowan models

The above results suggest that Wilson-Cowan models could successfully reproduce contrast response curves and masking, which have not been addressed through these models. Here we explicitly check this hypothesis.

We can use the proposed relation to plug successful parameters of Divisive Normalization fitted for contrast perception into the equivalent Wilson-Cowan model. We can avoid the integration of the differential equation using the knowledge of the steady state. The only problem to compute the response through the steady state solution is that the kernel of the Divisive Normalization depends on the (still unknown) response.

In this case we compute a first guess of the response, \hat{x} , using the fixed (signal-independent) hand-crafted kernel tuned in [11], and then, this first guess is used to compute the proposed signal-dependent kernel which in turn is used to compute the actual response, x . We consistently got compatible responses (e.g. $|x - x'|/|x| = 0.0022 \pm 0.0001$ over the TID dataset of natural images), so we used this method to compute the responses to synthetic patterns of controlled frequency and contrast.

Fig. 13 shows the results of the variations of the response of units tuned to low and high frequency tests as a function of the contrast of the tests located on top of backgrounds of different frequency and orientations. The results display the qualitative properties of masking: frequency, saturation, and cross effects (both in frequency and orientation).

4.2.4 Metric of the image space from the Wilson-Cowan model

As a result of consistency of the responses with the fixed and the adaptive kernels, the Wilson-Cowan model may also be used to predict subjective image distortion. In this section we explicitly check the performance of the Wilson-Cowan response to compute the visibility of distortions from neural differences (see Fig. 14)

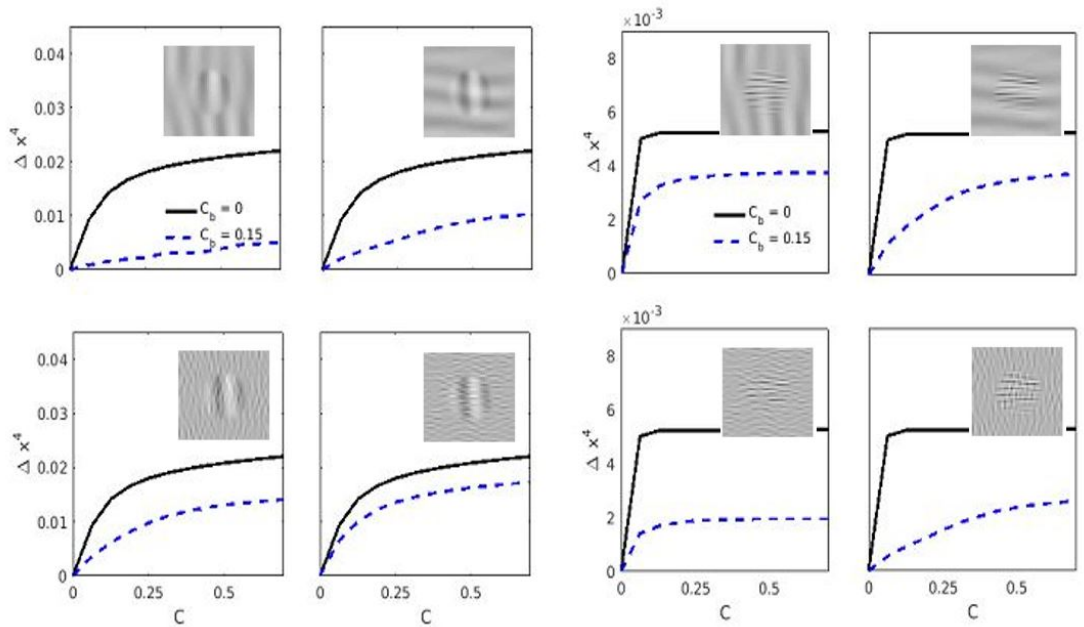


Fig 13. Contrast response curves for low frequency vertical tests (left) and high frequency horizontal tests (right) seen on top of backgrounds of different frequency, orientation and contrast. The images in the insets illustrate the kind of stimuli used in each simulation.

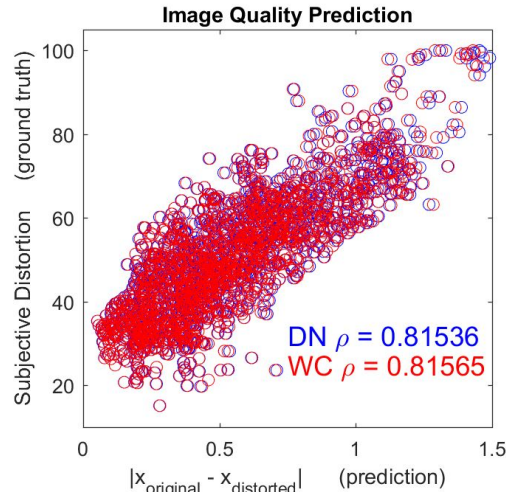


Fig 14. Prediction of subjective image distortion using Divisive Normalization and equivalent Wilson-Cowan.

5 Concluding remarks

The proposed relation implies (a) specific structure in the interaction kernel of divisive normalization. This structure explains the need of extra high-pass filters for unit-norm Gaussian interactions that are necessary to describe masking [11]. This kernel is signal dependent consistently with suggestions in [8]; (b) low-level Wilson-Cowan dynamics may also explain behavioral aspects that were classically explained through Divisive Normalization such as contrast response curves [3, 10] or image distortion metrics [20, 40]; and more importantly, (c) it allows to analyze Divisive Normalization in new ways that have been developed for Wilson-Cowan systems [22], as for instance the standard stability analysis that has been applied to the Divisive Normalization solution and confirms the steady-state assumption.

Acknowledgments.

This work was partially funded by the MINECO/FEDER/EU projects TEC2013-50520-EXP and BFU2014-59776-R, and TIN2015-71537-P; by the European Research Council, Starting Grant ref. 306337; and by the Icrea Academia Award.

References

1. Carandini M, Heeger DJ. Normalization as a canonical neural computation. *Nature Rev Neurosci.* 2012;13(1):51–62.
2. Hillis JM, Brainard DH. Do common mechanisms of adaptation mediate color discrimination and appearance? *JOSA A.* 2005;22(10):2090–2106.
3. Watson AB, Solomon JA. Model of visual contrast gain control and pattern masking. *JOSA A.* 1997;14(9):2379–2391.
4. Simoncelli EP, Heeger D. A Model of Neuronal Responses in Visual Area MT. *Vision Research.* 1998;38(5):743–761.
5. Sato T, Haider B, Hausser M, Carandini M. An excitatory basis for divisive normalization in visual cortex. *Nature Neuroscience.* 2016;19. doi:10.1038/nn.4249.
6. Schwartz O, Sejnowski TJ, Dayan P. Perceptual organization in the tilt illusion. *Journal of Vision.* 2009;9(4):19–19. doi:10.1167/9.4.19.
7. Schwartz G, Rieke F. Nonlinear spatial encoding by retinal ganglion cells: when $1 + 1 \neq 2$. *The Journal of General Physiology.* 2011;138(3):283–290. doi:10.1085/jgp.201110629.

-
8. Coen-Cagli R, Dayan P, Schwartz O. Cortical surround interactions and perceptual salience via natural scene statistics. *PLoS Computational Biology*. 2012;8(3). doi:10.1371/journal.pcbi.1002405.
 9. Coen-Cagli R, Schwartz O. The impact on midlevel vision of statistically optimal divisive normalization in V1. *Journal of Vision*. 2013;13(8):13.
 10. Malo J, Laparra V. Psychophysically tuned divisive normalization approximately factorizes the PDF of natural images. *Neural computation*. 2010;22(12):3179–3206.
 11. Martinez-Garcia M, Bertalmío M, Malo J. In Praise of Artifice Reloaded: Caution With Natural Image Databases in Modeling Vision. *Frontiers in Neuroscience*. 2019;13:8. doi:10.3389/fnins.2019.00008.
 12. Wilson HR, Cowan JD. Excitatory and inhibitory interactions in localized populations of model neurons. *Biophys J*. 1972;12:1–24.
 13. Wilson HR, Cowan JD. A mathematical theory of the functional dynamics of cortical and thalamic nervous tissue. *Kybernetik*. 1973;13(2):55–80. doi:10.1007/BF00288786.
 14. Amari Si. Dynamics of pattern formation in lateral-inhibition type neural fields. *Biological Cybernetics*. 1977;27(2):77–87. doi:10.1007/BF00337259.
 15. Wilson HR, Humanski R. Spatial frequency adaptation and contrast gain control. *Vision Research*. 1993;33(8):1133 – 1149. doi:https://doi.org/10.1016/0042-6989(93)90248-U.
 16. Bressloff P, Cowan J, Golubitsky M, Thomas P, C Wiener M. What Geometric Visual Hallucinations Tell Us about the Visual Cortex. *Neural computation*. 2002;14:473–91. doi:10.1162/089976602317250861.
 17. Bertalmio M. From image processing to computational neuroscience: A neural model based on histogram equalization. *Front Comput Neurosci*. 2014;8(71):1–7.
 18. Malo J, Epifanio I, Navarro R, Simoncelli EP. Nonlinear image representation for efficient perceptual coding. *IEEE Transactions on Image Processing*. 2006;15(1):68–80.
 19. Bertalmio M, Cyriac P, Batard T, Martinez-Garcia M, Malo J. The Wilson-Cowan model describes Contrast Response and Subjective Distortion. *J Vision*. 2017;17(10):657–657.
 20. Laparra V, Muñoz-Marí J, Malo J. Divisive normalization image quality metric revisited. *JOSA A*. 2010;27(4):852–864.
 21. Berardino A, Balle J, Laparra V, Simoncelli EP. Eigen-distortion of hierarchical representations. *Adv Neur Inf Proc NIPS-17*. 2017;.
 22. Destexhe A, Sejnowski TJ. The Wilson–Cowan model, 36 years later. *Biological Cybernetics*. 2009;101(1):1–2. doi:10.1007/s00422-009-0328-3.
 23. Cavanaugh JR. Properties of the Receptive Field Surround in Macaque Primary Visual Cortex. PhD Thesis, Center for Neural Science, New York Univ. 2000;.
 24. Cavanaugh JR, Bair W, Movshon JA. Selectivity and Spatial Distribution of Signals From the Receptive Field Surround in Macaque V1 Neurons. *Journal of Neurophysiology*. 2002;88(5):2547–2556. doi:10.1152/jn.00693.2001.
 25. USC-SIPI Image Database; 1977. <http://sipi.usc.edu/database/>.
 26. Martinez-Garcia M, Cyriac P, Batard T, Bertalmio M, Malo J. Derivatives and Inverse of Cascaded Linear+Nonlinear Neural Models. *PLoS ONE* 13(10): e0201326 <https://doi.org/10.1371/journal.pone.0201326>. 2018;.
 27. Chossat P, Faugeras O. Hyperbolic Planforms in Relation to Visual Edges and Textures Perception. *PLoS computational biology*. 2009;5:e1000625. doi:10.1371/journal.pcbi.1000625.
 28. Bressloff PC, Cowan JD. The functional geometry of local and horizontal connections in a model of V1. *Journal of Physiology-Paris*. 2003;97(2):221 – 236. doi:https://doi.org/10.1016/j.jphysparis.2003.09.017.
 29. Campbell FW, Robson JG. Application of Fourier Analysis to the Visibility of Gratings. *Journal of Physiology*. 1968;197:551–566.

-
30. Legge GE, Foley JM. Contrast Masking in Human Vision. *Journal of the Optical Society of America*. 1980;70:1458–1471.
 31. Legge GE. A Power Law for Contrast Discrimination. *Vision Research*. 1981;18:68–91.
 32. Foley JM. Human Luminance Pattern Mechanisms: Masking Experiments require a New Model. *Journal of the Optical Society of America A*. 1994;11(6):1710–1719.
 33. Schwartz O, Simoncelli EP. Natural signal statistics and sensory gain control. *Nature Neurosci*. 2001;4(8):819–825.
 34. Coen-Cagli R, Dayan P, Schwartz O. Cortical Surround Interactions and Perceptual Saliency via Natural Scene Statistics. *PLOS Computational Biology*. 2012;8(3):1–18. doi:10.1371/journal.pcbi.1002405.
 35. Malo J, Simoncelli E. Geometrical and statistical properties of vision models obtained via maximum differentiation. In: *SPIE Electronic Imaging*. International Society for Optics and Photonics; 2015. p. 93940L–93940L.
 36. Hateren JHv, Schaaf Avd. Independent Component Filters of Natural Images Compared with Simple Cells in Primary Visual Cortex. *Proceedings: Biological Sciences*. 1998;265(1394):359–366.
 37. Laparra V, Jiménez S, Camps-Valls G, Malo J. Nonlinearities and adaptation of color vision from sequential principal curves analysis. *Neural Computation*. 2012;24(10):2751–2788.
 38. Logan JD. *A First Course in Differential Equations*. 3rd ed. Springer Publishing Company, Incorporated; 2015.
 39. Simoncelli EP, Freeman WT, Adelson EH, Heeger DJ. Shiftable multi-scale transforms. *IEEE Trans Information Theory*. 1992;38(2):587–607. doi:10.1109/18.119725.
 40. Berardino A, Laparra V, Ballé J, Simoncelli EP. Eigen-Distortions of Hierarchical Representations. In: *Adv. Neur. Inf. Proc. Syst.* 30; 2017. p. 3533–3542.
 41. Wyszecki G, Stiles WS. *Color Science: Concepts and Methods, Quantitative Data and Formulae*. New York: John Wiley & Sons; 1982.
 42. Fairchild MD. *Color Appearance Models*. The Wiley-IS&T Series in Imaging Science and Technology. Wiley; 2013.
 43. Graham N. *Visual Pattern Analyzers*. Oxford University Press; 1989.

6 Supplementary Materials

6.1 High-pass filters in the kernel of Divisive Normalization

In this supplementary material we compare contrast response curves of two versions of the 4-layer model illustrated in Fig. 1 of the main text. In these models, the first three non-cortical layers were kept fixed (optimized as in [26]) and variations were introduced only in the last layer after the linear wavelet transform.

The top panel of Fig. 15 shows the parameters of the two Divisive Normalization transforms considered for the last cortical layer: the matrix at the left is the classical kernel \mathbf{H}^{ws} , and the matrix at the right is the modified kernel $\mathbf{H} = \mathbb{D}_l \cdot \mathbf{H}^{ws} \cdot \mathbb{D}_r$. The block-diagonal structure of these matrices comes from the vector organization of the wavelet coefficients in Simoncelli’s steerable pyramid [39]: scales are considered from fine to coarse; at each scale, each subband is spatially flattened column-wise, and the different orientations are considered in turn. Therefore, gray levels inside the diagonal blocks represent intraband Gaussian spatial interaction, and the off-diagonal block represent interactions between different orientations and scales. The parameters of \mathbf{H}^{ws} were selected in this way: the spatial width of the interaction came from fitting subjective image quality databases (as in [26] which used an intraband-only kernel), and the frequency and orientation widths were taken from [3].

The additional plots in the top panel of Fig. 15 show the semisaturation, \mathbf{b} , and the vectors, \mathbf{l} and \mathbf{r} , that eventually modify the unit-norm Gaussian kernel \mathbf{H}^{ws} . The structure of these vectors also comes from the conventional organization of the wavelet coefficients in [39]. The values of these vectors in the model at the left come from the optimization of a subjectively rated database [26], where they don’t introduce changes in the structure of \mathbf{H}^{ws} (only \mathbf{b} was optimized). On the contrary, in [11] (the model in the right panel), the values of these extra vectors were explicitly tuned: the vectors \mathbf{l} and \mathbf{r} in the right panel are *high-pass* filters because they have higher values for fine scales and lower values for coarse scales. That is why the blocks corresponding to the coarse scales are relatively attenuated in the modified kernel at the right.

This attenuation is critical to correct the relative failure of the unit-norm kernel model (at the left) with high-frequency tests.

In this simulation, the contrast response curves (the Δx^4 vs C plots at the bottom of Fig. 15) were computed increasing the contrast of the test pattern in the center of the images of the inset of the plots. Variations of responses of cells of the 4-th layer tuned to the corresponding tests are plotted as a function of the contrast of the test. The different line styles represent the responses when increasing the contrast of the background.

Both models (with kernels \mathbf{H}^{ws} and \mathbf{H} respectively) lead to bigger responses to low-frequency patterns, which is consistent with the Contrast Sensitivity Function. The nonlinearity for sensors tuned to low-frequency patterns is also qualitatively right in both models too: note that the response saturates, the decay increases with the contrast of the background, but the effect of high-frequency backgrounds is almost negligible.

However, normalization with \mathbf{H}^{ws} fails for high-frequency tests (curves highlighted in red circles): the impact of low-frequency backgrounds on high-frequency tests is bigger than the impact of high-frequency backgrounds, which is not compatible with actual contrast perception. That is why the structure of the classical unit-norm Gaussian kernel has to be modified.

In [11] we argue that automatic fitting the widths of the Gaussian kernel in large natural image databases may miss the required change in the kernel structure revealed by artificial stimuli. We also proposed a stabilization constant (the scaling vector \mathbf{k} in Eq. 2) that grants more freedom to explore the relevant parameters \mathbf{b} , \mathbf{l} , and \mathbf{r} for fixed widths in \mathbf{H}^{ws} .

With this freedom to explore, we tuned the vectors \mathbf{l} and \mathbf{r} by hand so that we could reduce the influence of the activity in low-frequency sensors on high frequency sensors and hence fix the problem highlighted in red at the left panel, while keeping the right behavior for low-frequency tests. Contrast response curves at the right panel show the results: responses for low-frequency tests stay the same, but responses of sensors tuned to high-frequencies are more insensitive to low-frequency backgrounds, and the decay in response is bigger for high-frequency backgrounds as it should be according to contrast perception (highlighted curves in green).

The *empirical* conclusion is that the unit-norm Gaussian kernel has to be modulated by two high-pass diagonal matrices: $\mathbf{H} = \mathbb{D}_l \cdot \mathbf{H}^{ws} \cdot \mathbb{D}_r$.

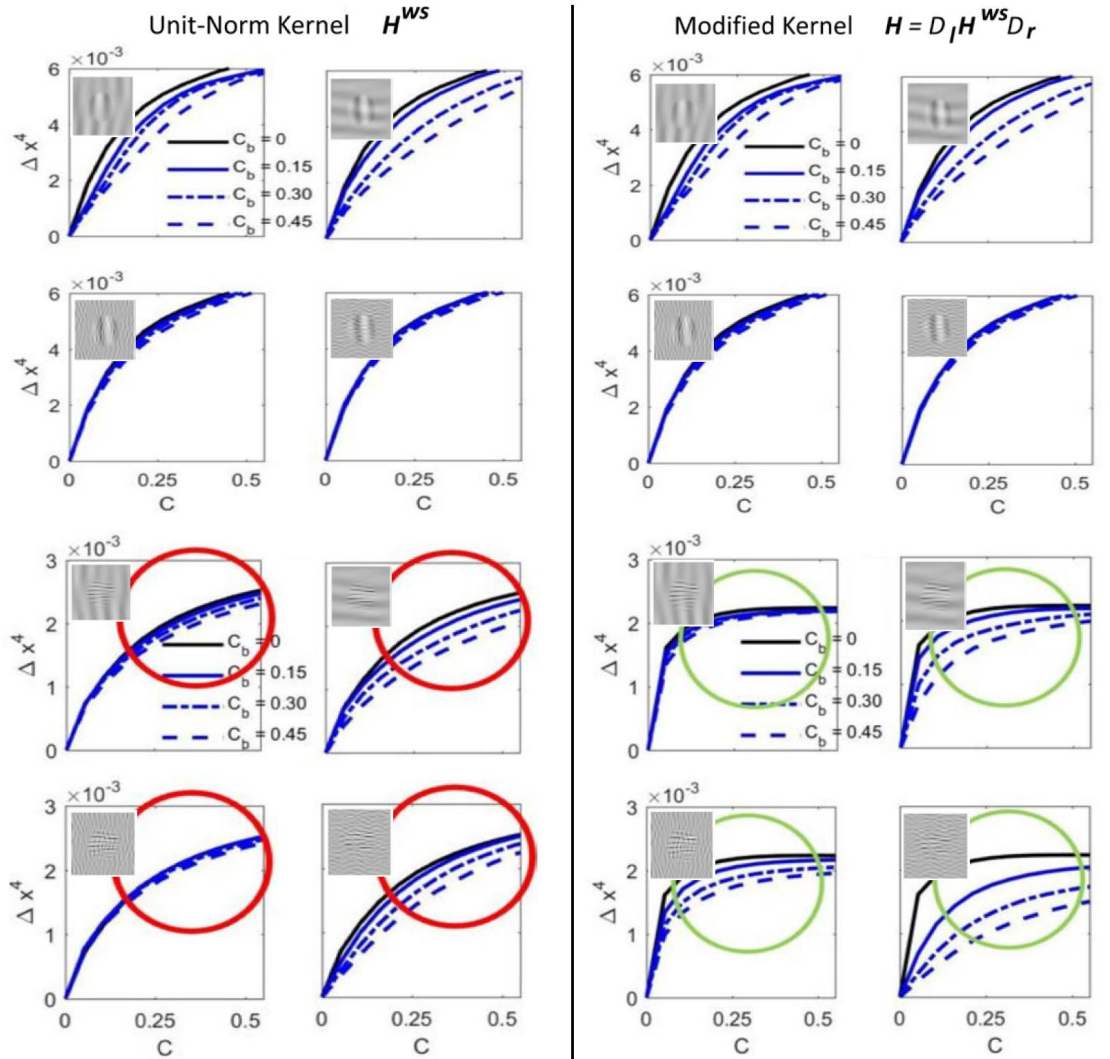
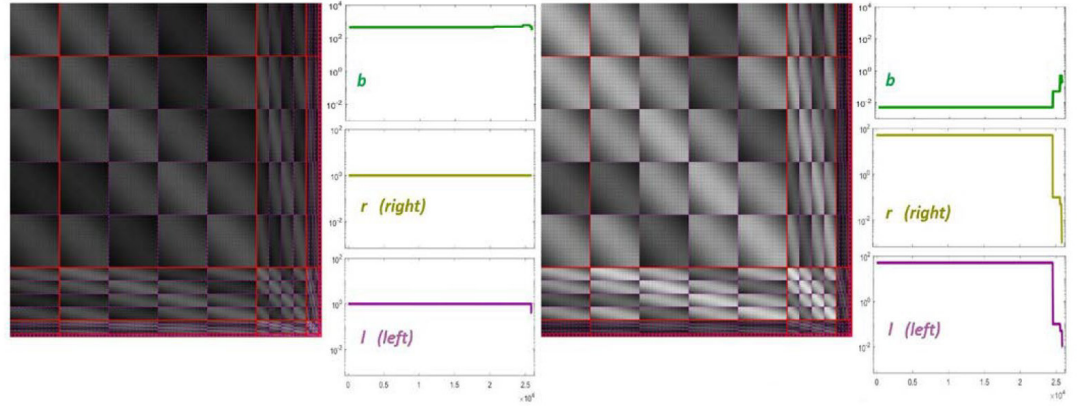


Fig 15. Structure of the interaction kernel in Divisive Normalization (adapted from [11]). This figure illustrates the differences between the classical unit-norm Gaussian kernel, H^{ws} (at the left), and the modified kernel that includes two extra high-pass diagonal matrices, $H = \mathbb{D}_l \cdot H^{ws} \cdot \mathbb{D}_r$ (at the right).

6.2 Illustrative small-scale Divisive Normalization system

In this Supplementary Material we consider a small-scale model with the basic cascaded linear+nonlinear structure that has been suggested for a number of perceptual modalities in neuroscience [1]. The interest of this example is that its analytical nature (fully studied in [11, 26]) and low dimensionality allows us to visualize the theoretical predictions on stability based on the Jacobian of the model.

6.2.0.1 The system Consider a system with only three photoreceptors acting on three-pixel images. Consider it is a cascade of just two L+NL layers,

$$\begin{array}{ccccccc}
 \mathbf{x}^0 & \xrightarrow{\mathcal{L}^{(1)}} & \mathbf{y}^1 & \xrightarrow{\mathcal{N}^{(1)}} & \mathbf{x}^1 & \xrightarrow{\mathcal{L}^{(2)}} & \mathbf{y}^2 & \xrightarrow{\mathcal{N}^{(2)}} & \mathbf{x}^2 \\
 & & & & \text{Layer 1} & & & & \text{Layer 2}
 \end{array} \tag{11}$$

where the first layer computes brightness in each spatial location and the next layer analyzes texture using spatial frequency sensors:

- Layer 1: brightness from radiance,

$$\begin{aligned}
 \mathcal{L}^{(1)} &\equiv \mathbf{y}^1 = V_\lambda \cdot \mathbf{x}^0 \\
 \mathcal{N}^{(1)} &\equiv \mathbf{x}^1 = (\mathbf{y}^1)^{\gamma_1}
 \end{aligned} \tag{12}$$

where $\gamma_1 < 1$.

- Layer 2: spatial frequency analyzers and contrast response,

$$\begin{aligned}
 \mathcal{L}^{(2)} &\equiv \mathbf{y}^2 = G \cdot F \cdot \mathbf{x}^1 \\
 \mathcal{N}^{(2)} &\equiv \mathbf{x}^2 = \text{sign}(\mathbf{y}^2) \odot \mathbf{k} \odot \frac{|\mathbf{y}^2|^{\gamma_2}}{\mathbf{b} + \mathbb{D}_l \cdot H^{ws} \cdot \mathbb{D}_r \cdot |\mathbf{y}^2|^{\gamma_2}}
 \end{aligned} \tag{13}$$

where the linear stage consists of a matrix F with three frequency-sensitive sensors tuned to textures of different spatial frequency,

$$F = \begin{pmatrix} 0.577 & 0.577 & 0.577 \\ 0.7071 & 0 & -0.707 \\ 0.408 & -0.817 & 0.408 \end{pmatrix}$$

and of a matrix G that sets the linear gain of each of these sensors:

$$G = \begin{pmatrix} 1 & 0 & 0 \\ 0 & 0.5 & 0 \\ 0 & 0 & 0.2 \end{pmatrix}$$

Finally, the energy in the nonlinear part is also mediated by a compressive exponent, $\gamma_2 < 1$, and the interaction matrix H^{ws} is:

$$H^{ws} = \begin{pmatrix} 1 & 0.3 & 0.1 \\ 0.3 & 1 & 0.3 \\ 0.1 & 0.3 & 1 \end{pmatrix}$$

modulated by two high pass filters: $\mathbf{l} = \mathbf{r} = (1, 0.5, 0.25)^\top$, with a semisaturation given by $\mathbf{b} = (0.10, 0.05, 0.02)^\top$, and global scaling given by $\mathbf{k} = (0.84, 0.08, 0.01)^\top$

The biological basis of this two-layer network is straightforward: integration over wavelengths is done using the standard spectral sensitivity function, V_λ , leading to the luminance [41], and we assume a simple, point-wise and fixed, exponential relation between luminance and brightness [41, 42]. Regarding spatial pattern analysis, we assume frequency-selective linear sensors [43] in the rows of F . The first sensor (first row) is tuned to the DC component of brightness, the second sensor (second row) to the low frequency component, and the last sensor (third row) to the high frequency. Each of these linear sensors has different (frequency

dependent) gain in the diagonal matrix G . This gain is low-pass, i.e. similar to the Contrast Sensitivity Function, CSF [29]. Finally, the contrast response undergoes a compressive transform where the interactions between coefficients are neglected as in [30,31]. This is equivalent to assuming an identity matrix as interaction kernel in Divisive Normalization in more sophisticated models [3, 11, 26].

As a result, the responses at the k -th *photo-receptor* of the first L+NL layer represent the *luminance*, z_k^1 , and the *brightness*, x_k^1 , at the k -th spatial location. Given the frequency analysis meaning of F , the responses z_1^2 and x_1^2 are related to the average brightness of the image, while z_k^2 and x_k^2 , with $k > 1$, are related to the amplitude or *contrast* of the low- and high-frequency AC components. With this in mind we will be able to identify the trends of biologically meaningful magnitudes from the proposed expressions in terms of the *luminance* and *contrast* of the images in the stimulus space. The nonlinearities of the second layer applied to the average brightness and to the low- and high-frequency components are illustrated in Fig. 16.

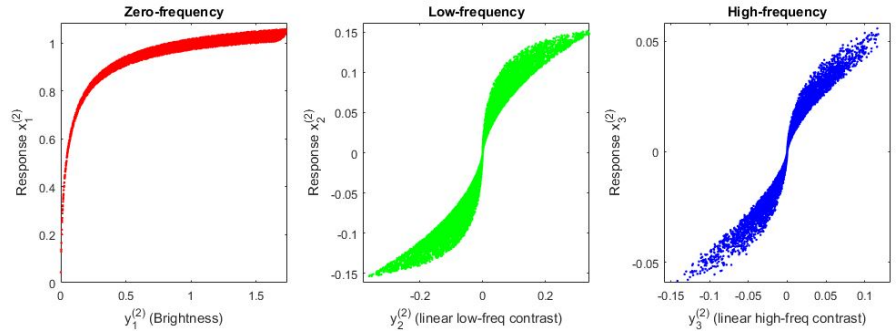


Fig 16. Nonlinearities of the second layer.